Seismic tremor at the 9°50′N East Pacific Rise eruption site

P. W. Monigle

Department of Marine, Earth and Atmospheric Sciences, North Carolina State University, Raleigh, North Carolina 27606, USA

Now at College of Oceanic and Atmospheric Sciences, Oregon State University, 104 COAS Admin Building, Corvallis, Oregon 97331, USA (pwmonigl@me.com)

D. R. Bohnenstiehl

Department of Marine, Earth and Atmospheric Sciences, North Carolina State University, Raleigh, North Carolina 27606, USA

M. Tolstoy and F. Waldhauser

Lamont–Doherty Earth Observatory, Earth Institute at Columbia University, 61 Route 9W, Palisades, New York 10964, USA

[1] Ocean bottom seismic observations within the 9°50′N region of the East Pacific Rise indicate persistent, low-amplitude tremor activity throughout the October 2003 through February 2007 period of monitoring. These signals exhibit either monochromatic or polychromatic spectral characteristics, with a ~6 Hz fundamental frequency and up to two harmonics. Individual events cannot be correlated between nearby (<1 km) stations, implying the presence of multiple, small-amplitude sources positioned within the shallow crust. Tremor exhibits a semidiurnal periodicity, with some stations recording activity during times of increasing tidal extension and others detecting tremor signals during times of increasing compression. The amplitude, duration, and rate of activity also correlate positively with fortnightly changes in the amplitude of the tides. These spatiotemporal patterns are consistent with tremor generation in response to tidally modulated fluid flow within a network of shallow cracks. Tremor energy flux is spatially and temporally heterogeneous; however, there are extended periods of greater and lesser activity that can be tracked across portions of the array. Despite their shallow crustal origin, changes in tremor amplitude and spectral character occur in the months prior to a major microearthquake swarm and inferred seafloor spreading event on 22 January 2006, with an increase in the degree of correlation between tremor activity and tidal strain in the weeks leading up to this event. After the spreading event, two eruption-surviving stations near the axis continue to show high rates of tremor activity, whereas these signals are suppressed at the single station recovered from the near-axis flanks. This off-axis quiescence may result from the dike-induced closing of cracks or perhaps from the emplacement of impermeable flows near the station.

Theme: Recent Volcanic Eruptions, Properties, and Behavior of the Fast Spreading East Pacific Rise at 8°−11°N
Guest Editors: S. M. Carbotte, R. Haymon, and W. Seyfried

1. Introduction

[2] Seismic tremor signals are sustained harmonic ground motions that have been described extensively in association with subaerial volcanoes. These signals, which often precede eruptions, have become an increasingly important monitoring tool in subaerial volcanic systems [*Konstantinou and Schlindwein*, 2003; *Chouet*, 2003; *McNutt*, 2005]. The mechanisms responsible for generating tremor in these environments are not well understood; however, a number of candidate processes have been put forth, including (1) fluid flow−induced oscillations [e.g., *Julian*, 1994], (2) the excitation and resonance of fluid-filled cracks [e.g., *Chouet*, 1988] or magma bodies [e.g., *Chouet*, 1996], and (3) the growth and collapse of fluid-filled bubbles due to hydrothermal boiling [e.g., *Leet*, 1988]. All of these mechanisms involve the interaction of magmatic or hydrothermal fluids with their surrounding host rocks.

[3] Tremor signals also have been reported in nonvolcanic settings. In some cases these signals can be linked similarly to the presence or movement of fluids or gas within a crustal reservoir. For example, the resonance of a water-CO_2 filled crack has been put forth to explain persistent tremor at shallow (<5 km) crustal depth in the central Apennines, Italy. These CO_2-rich fluids are proposed to originate from the degassing of mantle rocks at much greater depths [*Piccinini and Saccorotti*, 2008]. Elsewhere, within the fore-arc wedge offshore of Ecuador and Costa Rica, oscillating methane bubble clouds [*Pontoise and Hello*, 2002] and pulsed fluid release events [*Brown et al.*, 2005] have been suggested as mechanisms for generating harmonic signals with similar time-frequency characteristics.

[4] Harmonic tremor has even been observed in passive tectonic settings, such as the submerged portion of the Galicia margin in the northern Atlantic. *Díaz et al.* [2007] report a strong 6 h periodicity of these signals, suggesting they are driven by fluid pressure transients induced by ocean tidal loading. These quarter-diurnal peaks in tremor activity occur during the interval between high and low tide, often near the time when the strain rate induced by ocean tidal loading reaches a maximum [*Díaz et al.*, 2007].

[5] A separate class of nonvolcanic tremor has been observed at depth within some subduction zones [e.g., *Obara*, 2002]. Geodetic and seismic monitoring along both the Cascadia and Japanese margins indicates that tremor signals are generated preferentially during periods when a portion of the plate interface slips aseismically [*Miller et al.*, 2002; *Rogers and Dragert*, 2003; *Obara et al.*, 2004; *Shelly et al.*, 2007]. During these slip episodes, Coulomb stress changes associated with the solid Earth tides and ocean tidal loading have been shown to correlate with the timing of tremor activity [*Shelly et al.*, 2007; *Rubinstein et al.*, 2008; *Nakata et al.*, 2008]. This idea that relatively small ($10^{3−4}$ Pa) tidal stress changes may influence the timing of tremor-producing aseismic fault motions is an extension of the mechanism used to explain tidal triggering of seismogenic motions (earthquakes) within the shallow crust [e.g., *Tanaka et al.*, 2002; *Cochran et al.*, 2004; *Wilcock et al.*, 2001; *Tolstoy et al.*, 2002; *Stroup et al.*, 2007].

[6] Most relevant to this study are observations of tremor originating from submarine volcanic and hydrothermal systems in the deep ocean. Acoustic signals with harmonic characteristics have been detected at far regional distances by moored underwater hydrophones and island-based seismic stations [e.g., *Talandier and Okal*, 1987; *Dziak and Fox*, 2002; *Haxel and Dziak*, 2005]. These tremor signals appear to be sourced from shallow (<800 m) volcanic seamounts, where sound may couple into and propagate efficiently within the ocean's low-velocity waveguide. They commonly are interpreted to reflect resonance within the submarine magma chamber, and sometimes exhibit a repetitive pattern, suggesting a geyser-like process [*Talandier and Okal*, 1996].

[7] Local deployments of ocean bottom sensors also have recorded harmonic waveforms near the
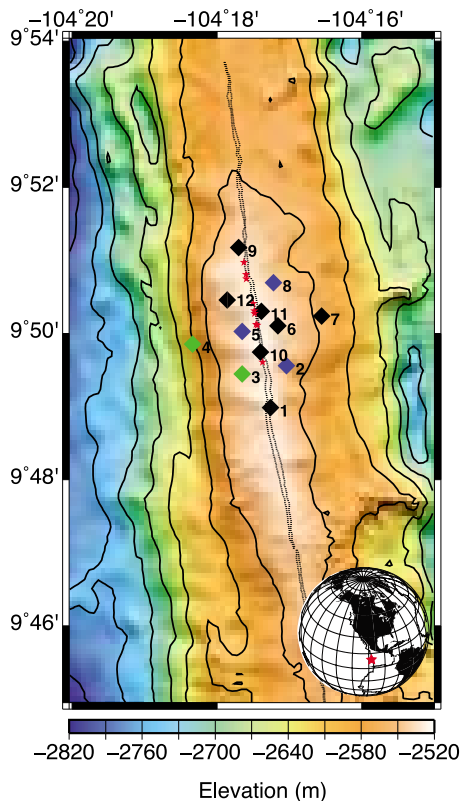
Figure 1. Locations of the 12 unique OBS stations along the ridge crest plotted along with locations of known high-temperature hydrothermal vent systems (red stars). Black diamonds denote stations dominated by tremor occurrence during periods of extensional strain. Green diamonds denote stations dominated by tremor occurrence during periods of compressional strain. Blue diamonds denote stations in which tremor occurrence is temporally nonrandom in both extensional and compressional strain regimes. The periods of active monitoring at each station are in Table 1. Gray lines denote the AST [*Fornari et al.*, 1998a].

summits of both Brothers Volcano in the Kermadec Arc [*Dziak et al.*, 2008] and Axial Volcano on the Juan de Fuca Ridge [*Tolstoy et al.*, 2002]. Although such signals have been described as pervasive, they typically cannot be correlated between nearby stations. This observation implies the existence of multiple shallow sources that may represent resonance within a network of fluid-filled cracks, rather than within the central magma chamber that underlies these volcanic systems [*Tolstoy et al.*, 2002; *Dziak et al.*, 2008].

[8] Beginning in October 2003, an array of ocean bottom seismometers (OBSs) was deployed locally along the crest of the East Pacific Rise (EPR) near 9°50′N. This project was part of a RIDGE 2000 initiative to monitor hydrothermal processes along

this fast spreading mid-ocean ridge (MOR) system. A catalog of discrete microearthquake events has been generated from the first 7 months of seismic monitoring [*Tolstoy et al.*, 2008]. These data have been used to define the pattern of hydrothermal flow within the crust [*Tolstoy et al.*, 2008], as well as delineate the size-frequency distribution [*Bohnenstiehl et al.*, 2008] and tidally influenced temporal pattern of microearthquakes [*Stroup et al.*, 2007].

[9] Here we report on harmonic tremor observed by this OBS array during its full 41 month period of monitoring between October 2003 and February 2007. This time window brackets a seismically detected seafloor spreading event on 22 January 2006 [*Tolstoy et al.*, 2006]. Our focus is on documenting the pattern of tremor occurrence and changes in its rate and character that may be related to both dynamic tidal strains and the static magma-induced deformation. Such documentation provides a rare opportunity to examine the long-term evolution of tremor activity within a dynamic mid-ocean ridge system and investigate what role tremor detection might play in efforts to predict future eruptive activity in the deep ocean.

2. Study Site

[10] This study documents tremor activity recorded at a depth of ~2500 m along the fast spreading (110 mm/yr) EPR, between ~9°49 and 9°52′N latitude (Figure 1). The area exhibits an axial high morphology, with a 50–200 m wide and 5–20 m deep axial summit trough (AST) running along its crest [*Haymon et al.*, 1991; *Fornari et al.*, 1998a]. Multichannel seismic (MCS) investigations during the mid-1980s detected an axial magma chamber (AMC) reflector at ~1.4 km below the seafloor [*Kent et al.*, 1993], and preliminary analysis of 3-D MCS data collected during the summer of 2008 indicates that a pool of melt persists beneath the site [*Carton et al.*, 2008]. This long-lived magmatic system supports an active hydrothermal cell and the release of high- and low-temperature vent fluids at numerous sites along the ridge crest (Figure 1).

[11] The area near 9°50′N has been studied in detail since the immediate aftermath of a seafloor eruption was documented during a series of submersible dives in early 1991 [*Haymon et al.*, 1993]. Subsequent analysis of geochemical markers suggested that observations made by *Haymon et al.* [1993] occurred with a month of the eruption's cessation, with ^{210}Po-^{210}Pb dating of the young

lavas indicating the area was repaved by a series of eruptions during the course of a year [*Rubin et al.*, 1994]. Time series investigations since the 1991–1992 eruptive episode have focused on tracking the pattern of biological succession [*Shank et al.*, 1998], as well as documenting long-term changes in hydrothermal fluid temperature [*Fornari et al.*, 1998b; *Scheirer et al.*, 2006] and chemistry [*Von Damm et al.*, 1995].

[12] A previous OBS investigation by *Sohn et al.* [1998, 1999] recorded 283 microearthquakes beneath the 9°50′N area during a 3 month period in 1995. These results indicated a concentration of cracking within the hydrothermal reservoir, where the convective mining of heat from the upper crust results in a high rate of thermal stressing. This study also elucidated the possible impact of microearthquake activity on the hydrothermal system, documenting a vent temperature perturbation of nearly +7°C that correlated spatially and temporally with a swarm of activity within the subsurface. *Sohn et al.* [1998, 1999] did not report on the occurrence of tremor activity; however, inspection of their data set has revealed signals similar to those described here.

[13] The OBS data used in this study were collected during a series of four deployments between October 2003 and February 2007. Microearthquake arrivals from the first deployment (October 2003 to April 2004) have been carefully analyzed to produce a catalog of more than 9,000 earthquakes [*Tolstoy et al.*, 2008; *Bohnenstiehl et al.*, 2008]. Precisely relocated hypocenters, obtained using the double-difference procedure of *Waldhauser and Ellsworth* [2000], indicate a concentration of microearthquakes occupying a 200–300 m wide zone that lies at a depth of 0.9–1.4 km beneath the AST [*Tolstoy et al.*, 2008]. At shallow depths, *Tolstoy et al.* [2008] have documented a subvertical, pipe-like zone of microearthquake activity that is coincident with a 100 m offset in the AST near 9°49.25′N. This is interpreted to represent an on-axis down-flow zone, where cold seawater is being entrained into the crust [*Tolstoy et al.*, 2008].

[14] *Stroup et al.* [2007] has used this microearthquake catalog to show an increased rate of seismic activity during times of tidally induced extension, with volumetric stress changes of 0.7–4.0 kPa producing a nonrandom temporal behavior. As the region exhibits small (<0.2 m) ocean tides, these stress changes are modulated largely by the direct solid Earth tide. However, the spatial pattern of microearthquake phase lags relative to times of peak tidal extension may require an additional poroelastic

effect that indicates high permeabilities within the interfered down flow zone and beneath the main vent field near 9°50′N [*Stroup et al.*, 2009].

[15] Relative to seismic rates observed during the fall of 2003, when OBS monitoring began, there is a long-term ramp-up in microearthquake activity that culminates in a massive seismic swarm on 22 January 2006. *Tolstoy et al.* [2006] interpreted this swarm as marking the emplacement of a dike feeding a significant eruption within the site, an observation supported by regional hydrophone recordings [*Dziak et al.*, 2009]. Microseismicity rates drop dramatically in the day and weeks following the January 2006 seismic swarm [*Tolstoy et al.*, 2006].

[16] Subsequent water column and seafloor observations have confirmed the presence of recent volcanism, with approximately 22×10^6 m³ of lava erupted onto the seabed, or <15% of the total magma available in the AMC [*Soule et al.*, 2007]. Short half-life (^{210}Po-^{210}Pb) dating suggests eruptive activity beginning in June or July 2005 and terminating by January 2006, with approximately 80% of lava extruded by September 2005 [*Rubin et al.*, 2008]. However, this observation remains at odds with both local OBS [*Tolstoy et al.*, 2006] and regional hydroacoustic observations [*Dziak et al.*, 2009], which indicate that the site's seismic energy release is dominated by the single swarm event on 22 January 2006.

3. Tremor Character

[17] Seismic activity along the 9°50′N ridge crest is characterized by both discrete local earthquake activity and seismic tremor. Local microearthquake activity is broadband and transient, with typically short (<2–3 s) duration wave packets consisting of distinct P and S phase arrivals [*Tolstoy et al.*, 2008]. Tremor activity, however, represent a narrowband signal with a monochromatic or polychromatic spectral signature (Figure 2). Individual tremor packets typically extend for 10–100s of seconds (mean of 97 s, median of 57 s) and may occur in episodes lasting several hours. Although some tremor activity appears to be excited or amplified by the release of broadband energy during microearthquake events, tremor signals are most commonly observed as emergent waveforms that lack distinct phase arrivals (Figure 2).

[18] The occurrence rate and amplitude of tremor signals are spatially heterogeneous throughout the array (Table 1). This pattern may reflect the distri-
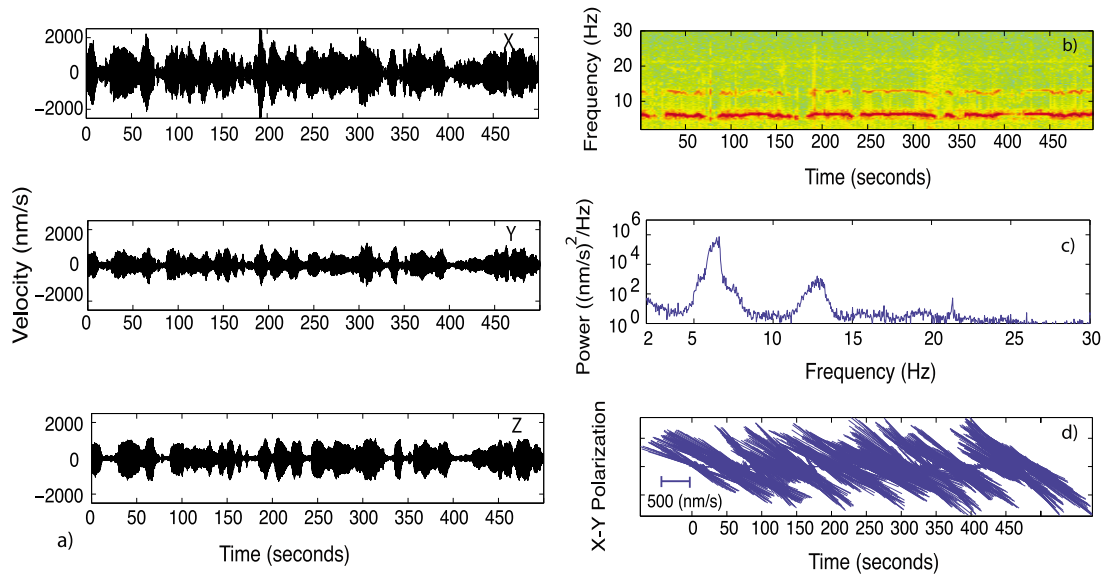
Figure 2. A typical tremor event recorded on OBS stations. Spectra were recorded at station 4 (deployment 3) on 4 May 2005 at 2047:28 UT. (a) X, Y, and Z components of seismic signal. (b) Spectral signature of tremor with fundamental frequency near 6 Hz and harmonic near 12 Hz. Spectrogram parameters are hamming window length of 512 samples with a 256 sample overlap, using 512 frequency points in the Fourier transform at a sampling frequency of 125 Hz. (c) Spectral power ($(nm/s)^2$/Hz) for 500 s window shown in spectrogram using Welch's method averaging eight windows with 50% overlap and 4096 points in the zero-padded FFT. (d) The instantaneous polarization on the X-Y plane in time.

bution and character of the tremor sources, as well as possible differences in the degree of coupling among these drop-deployed sensors. In general, however, tremor occurrence and duration are greatest immediately along the ridge crest (stations 1 and 9–11) (Table 1 and Figure 1).

[19] Specific packets of tremor activity cannot be correlated between stations within the array, preventing their locations from being determined and suggesting that multiple small-amplitude sources occur near each station. As the smallest distance between instruments is approximately 0.55 km (between stations 6 and 11) and the average spacing is 1.75 km, this would suggest that tremor sources are located within a few hundred meters individual seismometers. Despite the incoherent character of these signals, periods of increasing and decreasing activity can be seen across the array. This pattern implies that these discrete local sources are sensitive to array-scale processes.

[20] A given packet of tremor commonly shows a consistent polarization signature (Figure 2), and for most stations the polarization remains stable during the deployment, being dominated by signals arriving from one or two azimuthal directions. These azimuths do not align to a common location, again suggesting the presence of distinct source regions near each station (Figure 3).

[21] The fundamental frequency of the observed tremor signals lies between 4 and 8 Hz. At individual stations, short-term fluctuations in frequency content occur over time scales ranging from 10s of seconds to minutes. This phenomenon, known as spectral gliding, may result from changing boundary conditions, which can include the dimensions of the resonating conduit and/or fluid flow rate [e.g., *McNutt*, 2005]. There are no sustained differences in frequency between stations or long-term trends throughout the monitoring period. One or two harmonics are commonly observed, with monochromatic signals evolving into polychromatic signals, or vice versa.

[22] Although ocean bottom currents are known to produce tidally correlated noise, inspection of near-bottom (10 m) acoustic Doppler current profiler (ADCP) data shows modest median velocities of 2.3 cm/s on axis (9° 50.54′N, 104° 17.52′W) and 3.5 cm/s off axis (9° 50.36′N, 104° 18.57′W, near station 4) [*Adams and Mullineaux*, 2008]. Moreover, measured current velocities only briefly exceed the ∼10 cm/s threshold for Karman vortex shredding, which has been shown to produce strong narrowband signals for some OBS configurations [e.g., *Duennebier et al.*, 1981]. The ADCP and seismic time series also exhibit low spectral coherence at semidiurnal periods and a significant quarter-diurnal spectral peak is seen in the off-axis

Table 1. Tremor Detection Data and Statistics

Stations	Start Day (Year, Day of Year)	End Day (Year, Day of Year)	Total Events	Total Tremor Duration (hours)	Tremor Duration (d/yr)	Mean Events per Hour	Median Amplitude (nm/s)	Mean Energy Density Flux (dB (nm²/s)/d)	Mean Phase	βcdf 90–180[a]	βcdf 270–360[a]
Deployment 1											
1	2003, 274	2004, 111	12106	310.33	23.48	2.44	211.60	87.36	317	R	X
2	2003, 274	2004, 111	5999	109.79	8.31	1.18	497.38	88.45	352	R	X
4	2003, 274	2004, 111	1798	27.86	2.11	0.33	24.03	55.92	123	X	R
7	2003, 275	2004, 113	5957	110.29	8.43	1.10	579.49	89.44	314	R	X
9	2003, 275	2004, 114	8073	180.36	13.71	1.73	332.71	87.99	317	R	X
Total			6787 (mean)	738.63	11.21 (mean)	1.36	329.04	81.83			
Deployment 2											
1	2004, 103	2005, 126	240	2.71	0.11	0.02	63.24	54.64	132	X	R
2	2004, 103	2005, 125	6162	107.57	4.23	0.64	225.00	80.41	319	X	X
3	2004, 103	2005, 125	13797	387.01	15.21	1.41	76.60	83.81	154	X	R
4	2004, 103	2005, 076	42	0.52	0.02	0.00	52.69	45.60	252	R	X
6	2004, 102	2005, 125	2422	37.98	1.49	0.24	36.61	58.14	331	R	X
8	2004, 104	2005, 127	12145	261.61	10.25	1.30	476.40	97.46	338	R	X
9[b]	2004, 110	2005, 070	3617	93.48	5.02	0.50	170.43	79.25	309	R	X
10	2004, 101	2005, 125	2743	33.95	1.33	0.28	30.27	58.96	323	R	X
11	2004, 101	2005, 127	13542	320.63	12.47	1.38	308.78	102.98	326	R	X
Total			6079 (mean)	1245.46	5.57 (mean)	0.64	160.00	73.47			
Deployment 3											
4	2005, 123	2006, 115	6705	158.71	6.86	0.76	421.94	89.67	132	X	R
4-pre	2005, 123	2006, 022	6564	156.54	9.05	1.04	439.73	90.95	130	X	R
4-post	2006, 023	2006, 115	141	2.17	0.36	0.06	89.01	58.88	151	X	R
5[b]	2005, 123	2006, 115	11664	337.39	19.36	1.82	251.27	89.86	274	X	X
5-pre[b]	2005, 123	2006, 022	7030	208.99	17.56	1.67	266.71	90.96	275	X	X
5-post	2006, 023	2006, 115	4634	128.40	21.69	2.15	237.85	86.34	271	X	X
9	2005, 121	2006, 114	15359	591.74	25.35	1.68	842.75	104.90	300	R	X
9-pre	2005, 121	2006, 022	11977	469.50	27.05	1.88	896.79	106.02	301	R	X
9-post	2006, 023	2006, 114	3382	122.25	21.13	1.56	768.10	96.10	273	X	X
Total			11242 (mean)	1087.84	17.19 (mean)	1.42	505.32	94.81			
Deployment 4											
1	2006, 114	2007, 014	3060	51.72	2.98	0.52	410.00	87.55	330	R	X
4	2006, 114	2007, 033	4323	111.88	6.01	0.55	309.28	85.32	176	X	X
7	2006, 114	2007, 032	12423	311.49	16.80	1.77	185.24	83.52	299	R	X
8	2006, 114	2007, 033	9557	210.49	11.31	1.36	134.83	78.44	317	X	X
10	2006, 114	2007, 032	14402	701.82	37.85	2.09	366.30	100.76	342	R	X
11	2006, 114	2007, 032	14482	404.61	21.82	2.09	364.61	89.68	355	R	X
12	2006, 114	2007, 033	4392	129.83	6.98	0.61	575.32	89.33	282	R	X
Total			8948 (mean)	1921.84	14.82 (mean)	1.28	335.08	87.80			

Table 1. (continued)

Stations	Start Day (Year, Day of Year)	End Day (Year, Day of Year)	Total Events	Total Tremor Duration (hours)	Tremor Duration (d/yr)	Mean Events per Hour	Median Amplitude (nm/s)	Mean Energy Density Flux (dB (nm²/s)/d)	Mean Phase	βcdf 90–180[a]	βcdf 270–360[a]
All Deployments											
4	2003, 274	2007, 033	11605	298.97	15.00	0.40	201.98	69.13	139	X	R
9	2003, 275	2006, 114	27049	865.58	44.09	1.30	448.63	90.71	307	R	X
Composite	2003, 274	2007, 033	7713 (mean)	4993.77	10.90 (mean)	1.08	289.45	82.06	319	X	X

[a] X indicates a temporally nonrandom occurrence (>99% significance), and R indicates a temporally random occurrence (>99% significance).
[b] Did not record continuously.

current meter records is not observed in the 4–8 Hz seismic band. Below we describe changes in the harmonic character, amplitude and rate of tremor occurrence that can be correlated with geologic activity within the region, making a strong case for their geologic origin.

4. Methods

4.1. OBS Data

[23] Four deployments of OBS instrumentation provide nearly continuous monitoring of the 9°50′N vent field between October 2003 and February 2007 (Figure 1). All instruments were drop deployed, with their positions on the seabed determined by acoustic ranging relative to the surface ship. The instrumentation deployed during the first deployment (October 2003 to April 2004) consisted of a short-period (Mark Products L22) seismic sensor and an omnidirection hydrophone. The second deployment (April 2004 to May 2005) collected only vertical channel, short-period seismic data (L22), and the third (May 2005 to April 2006) and fourth (April 2006 to February 2007) deployments were equipped with three-component short-period seismic sensors (Mark Products L28). As it is common to all deployments, we focus our analysis on data from the short-period, vertical channel.

[24] Figure 1 shows the twelve unique stations occupied during one or more of the deployments, with the time history of deployment at each station summarized in Table 1. Deployment 3 captured the eruptive activity, with many of the instruments engulfed by the fresh lava. Consequently, usable waveform data are available for only three of the seven instruments originally deployed (stations 4, 5 and 9), with intermittent recordings at station 5 and limited horizontal component data from station 9. The four deployments overlap minimally in time and space; however, there are no individual stations with a continuous record of activity throughout the monitoring period. Stations 4 and 9 represent the most complete records, as they were occupied during the first three deployments with only minor interruption. We limit our discussion of signal polarization (three-component data) to deployment four.

4.2. Tremor Detection

[25] To examine the temporal pattern of tremor recorded on each OBS, the root-mean-square (RMS) amplitudes of the response-corrected waveforms are calculated within the 4–8 Hz frequency
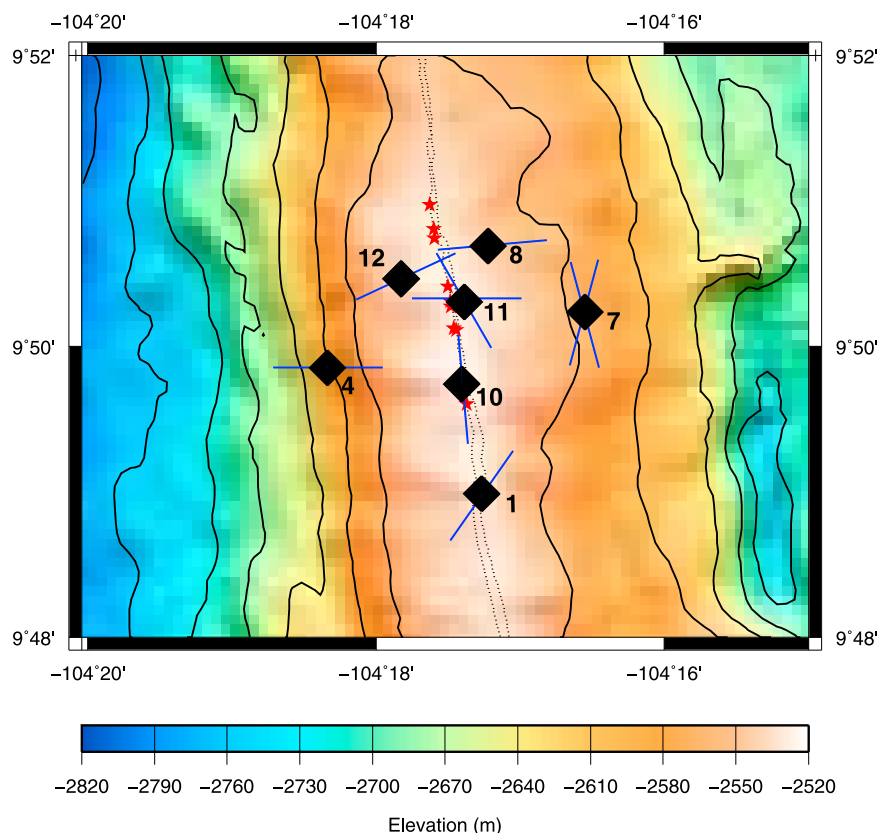
Figure 3. Polarization results for all fourth deployment stations. Station orientations determined from the analysis of regional earthquake signals. Stations 7 and 11 exhibit two dominant polarization azimuths. Red stars represent locations of known high-temperature hydrothermal vent systems, and gray lines denote the AST [*Fornari et al.*, 1998a].

band. This analysis is performed using the vertical component data, which are common to all instruments. RMS amplitudes are estimated within 10 min time windows that are nonoverlapping. This is similar to the approach used to quantify tremor activity in terrestrial volcanic systems [e.g., *Endo and Murray*, 1991]. However, as the observed tremor signals cannot be correlated between stations, no source locations are determined and distance-corrected displacements cannot be estimated.

[26] While waveform amplitudes within the 4–8 Hz band appear to be dominated by tremor activity, there are additional contributions from transient broadband signals, chiefly local earthquakes [*Tolstoy et al.*, 2008] and regional T waves [*Fox et al.*, 2001]. To better isolate tremor activity and detect individual "events," the spectrogram cross-correlation method of *Mellinger and Clark* [2000] is applied to the data set. This is implemented using the software package Ishmael, originally developed for bioacoustics [*Mellinger*, 2001].

[27] A hat-shaped detection kernel is defined as a function of frequency (Figure 4). The kernel is zero-sum, with positive amplitudes assigned within the tremor band (4–8 Hz) and equal regions of negative amplitude assigned to adjacent frequencies. Cross-correlating the kernel with the signal spectrogram generates a time series of recognition scores, representing the closeness of match between the tremor and the kernel. Due to the zero-sum nature of the kernel, a correlation of zero is returned for uniform background noise, as the positively and negatively correlated portions of the spectrogram exactly cancel. Similarly, nonuniform broadband signals return lower scores than tremor events (Figure 4). Setting the duration of the kernel at 25 s, ~180,000 tremor events totaling 208.15 days of tremor were detected on 24 instruments deployed at 12 unique stations (Table 1). The start and end times of each tremor are recorded, along with its RMS amplitude within the 4–8 Hz frequency band.

[28] Tremor energy flux density (E) also was calculated for each Ishmael-detected tremor event. Following *Madsen* [2005], $E \approx \int V_{RMS}^2 dt$, where T is the tremor duration in seconds and V_{RMS} is its RMS velocity amplitude. The summed energy flux density observed at a subset of the stations is shown
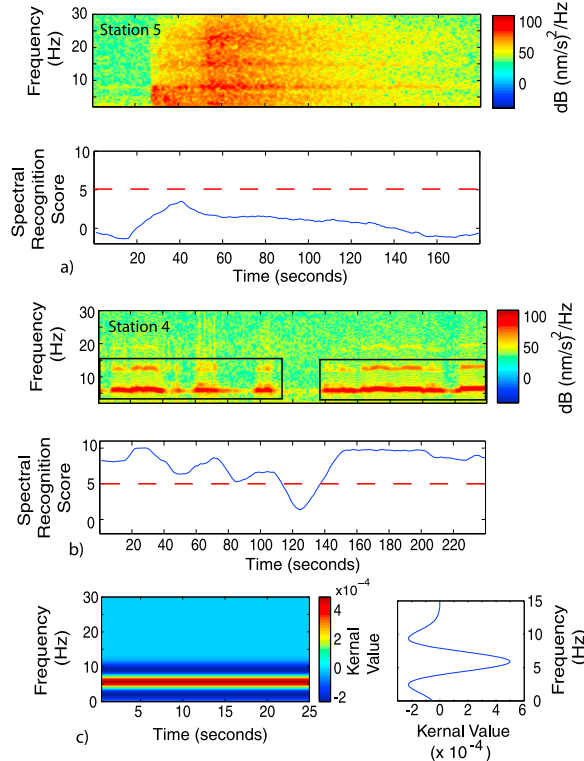
Figure 4. Spectrograms showing (a) a broadband arrival (P, S, and T phases) from a regional earthquake and (b) that of a 4–8 Hz tremor signal. (c) Cross correlation of a 25 s duration, hat-shaped kernel produces a time series of recognition scores. A detection threshold (red line) is then applied to create a series of detections.

in Figure 5. It has been calculated within 4 day windows, with 2 days of overlap between windows. Deployment-long average daily energy flux densities for each station are shown as horizontal bars in Figure 5, with deployment 3 further divided into pre– and post– 22 January 2006 average activity.

4.3. Assessment of Tidal Correlation

[29] Tidal strain was modeled using the GOTIC2 software [*Matsumoto et al.*, 2001], which predicts both the solid Earth and ocean tidal loading (OTL) components. Unless otherwise noted, the term tidal strain will refer to the combined effects of the solid Earth tide and OTL. Positive strains indicate extension.

[30] The effects of ocean loading are estimated by convolving the NAO.99b ocean tide model [*Matsumoto et al.*, 2000] with the Green's functions defined from a unit point mass acting on the Earth's surface [*Farrell*, 1972]. The calculations presented in this paper utilize the 21 major long- and short-period tidal constituents within NAO.99b. During

the period between April 2006 and January 2007, an ocean bottom pressure gauge also was deployed at the site (http://www.mgds.org: Cruise: AT15−26). A comparison of these data with the predicted bottom pressure time series based on the NAO.99b model shows that the two data sets agree in both phase and amplitude, with only minor offsets that can be accounted for by atmospheric pressure variations.

[31] Tidal strains exhibit a semidiurnal periodicity in the 9°50′N area, reaching maximum zero-to-peak strain amplitudes of 3×10^{-8} during spring tide. This strain corresponds to a volumetric stress change of $\sim \pm 2.5$ kPa (assuming a crust with Vp = 6.5 km/s, Vs = 3.5 km/s, $p = 2800$ kg/m³). Because ocean tidal (sea surface) heights near 9°50′N rarely exceed 20 cm, this deformation is controlled largely by the effects of the solid Earth tide, with the time of peak crustal extension occurring approximately 1 h after the peak in ocean tidal height [*Stroup et al.*, 2007].

[32] In order to evaluate the timing of tremor activity with respect to the tides, phase angles were assigned using the start time of each Ishmael-detected event. Troughs in the tidal strain time series (times of maximum volumetric compression) were assigned values of 180°, whereas peaks in the time series (time of maximum volumetric extension) were assigned values of 0° or 360° (Figure 6). Peaks and troughs were identified using a second derivative test, with phase assignments made using a linear interpolation within each half-cycle (following *Tanaka et al.* [2002]).

[33] Two statistical methods are implemented to assess the tidal phase distributions. First, the Schuster test is used to evaluate the probability (p) that the tremor phase angles are randomly distributed about the unit circle [*Emter*, 1997]. This method has been widely used in evaluating the tidal triggering of discrete earthquake events [e.g., *Tolstoy et al.*, 2002; *Wilcock et al.*, 2001; *Cochran et al.*, 2004; *Stroup et al.*, 2007]. The p value is calculated as: p = exp (−R²/N), where, R is the sum of the unit phasors representing the direction of each phase angle and N is the total number of tremor detections.

[34] The number of tremor events within each quadrant also is tested against a binomial model that assumes a randomly occurring event has a 1:4 chance of falling within a given 90° phase window. This is accomplished by evaluating the probability of obtaining $\geq$ N successes (tremors) in a given quadrant for a population of T trials: p = $1 - \beta_{cdf}$
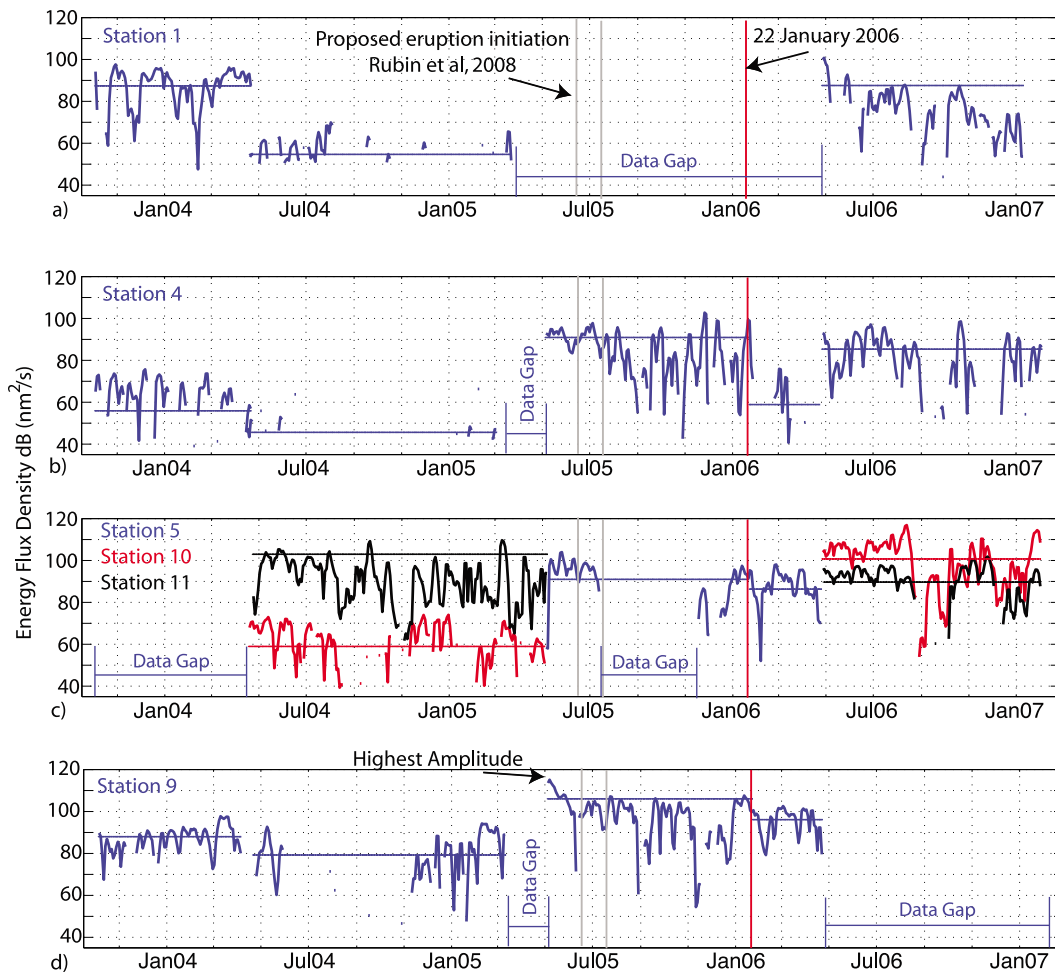
Figure 5. Energy flux density (dB (nm²/s)) within Ishmael-detected tremor events integrated over 4 day windows with 50% overlap. Stations (a) 1, (b) 4, (c) 5, and (d) 9. The date of the 22 January 2006 seismic swarm is denoted with a red line. *Rubin et al.*'s [2008] proposed period of eruption initiation based on ²¹⁰Po-²¹⁰Pb data is marked with gray lines. Station 5 recorded the eruption but was not occupied at any other time. As a result, stations 10 and 11 are included in the plot for comparison purposes, as these are the stations in closest proximity to station 5. The highest energy flux is observed at station 9 in May 2005. Horizontal bars represent average energy flux for days with tremor and also indicate the extent of the instrument deployment. Stations recording the eruption are further divided into averages before and after 22 January 2006. Periods without data between deployments as well as gaps in data coverage within deployments are labeled.

(N, T, 0.25), where β_{cdf} represent the cumulative distribution function for a binomial model evaluated for a probability of 0.25. For both the binomial and Schuster tests, p values ≤ 0.05 typically are adopted as significant [e.g., *Emter*, 1997; *Cochran et al.*, 2004; *Stroup et al.*, 2007].

5. Data Analysis and Observations

5.1. Tidal Correlation

[35] A semidiurnal periodicity in tremor occurrence commonly can be observed when plotting the 4–8 Hz band-passed RMS amplitudes versus time. An example is shown in Figure 7a, using data

from a period of pronounced tremor activity between 15 and 19 January 2006. GOTIC2-predicted tidal strain is shown in red. During this time, strain can be seen to peak ~2 h after the peak in RMS values (Figure 7a). Fast Fourier transforms (FFT) of the tidal strain and RMS time series (Figure 7b) reveal that both exhibit peak power at a frequency of 2 cycles/d. Cross-spectral analysis of these two signals indicates a correlation coefficient of 0.91 at this frequency, with a phase lag of $-57°$ obtained from coherence analysis (Figure 7c).

[36] Tremor events detected using the methods of *Mellinger and Clark* [2000] also are shown in Figure 7a. These detections occur during times of
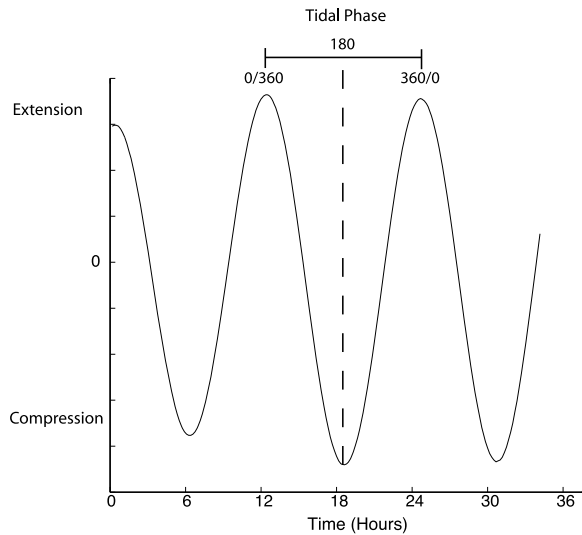
Figure 6. Illustration of a 36 h window of the tidal strain time series. The tidal phase of each individual tremor detection is determined by assigning a phase angle based on the start time of the tremor event. Phase angles are assigned based on 180° as the peak in compressional strain for a given tidal cycle, with 0° or 360° denoting the peak in extensional strain. Phase is assigned independent of strain value.

elevated RMS amplitude, implying that the amplitude of the band-passed RMS time series (Figure 7a) is responding to narrowband (tremor) signals, rather than broadband noise. The tremor detections shown in this example occur primarily during periods when the crust is extending (increasing strain), most often in the 270–360° quadrant (Figure 7d). The mean resultant phase angle of this tremor is $307 \pm 5.13°$ $(1 - \sigma)$, implying that tremor signals lag the time of peak tidal extension by $-53°$ on average. This agrees well with the $-57°$ lag determined through spectral coherence measurements.

[37] The methods illustrated in Figure 7 have been applied to all available data between October 2003 and February 2007. In implementing the cross-spectral analysis (Figure 7c), tidal strain was cross-correlated with RMS amplitude within 4 day windows that overlapped by 2 days. The phase lag was recorded for each 4 day window that exhibited a correlation value >0.5 at a frequency of 2 cycles/d.

[38] Application of the Schuster test indicates that tremor detections at all stations are nonrandomly distributed with respect to tidal phase (p values < 0.001). Both the distribution of tremor phase events and the cross-spectral results indicate a peak in tremor activity within either the 270–360° or 90–180° quadrant, or a bimodal distribution with

significantly nonrandom peaks in both quadrants (Figure 8). This implies tremor signals may be generated preferentially during times when the crust is dilating in response to the solid Earth tide (and ocean tide is high) or during times when the crust is compressing (and ocean tide is low).

[39] The probability of randomly recording $\geq$ N tremors in a given quadrant is quantified further using the binomial model (section 4.3) and the results are given in Table 1, with "X" representing temporally nonrandom behavior. Combining available data from all four deployments, stations 3 and 4 on the near-axis eastern ridge flanks show activity dominantly during periods of increasing compressive tidal strain (90–180°). Stations 1, 6–7, and 9–12 are characterized by tremor occurrence preferentially during times of increasing extension (270–360°) and all other stations show a significantly nonrandom number of events within both quadrants. For this latter group of sites, the correlation is observed to switch modes through time, typically following some period with a low rate of tremor activity. Hence, there is no pronounced 6 h periodicity, as reported by *Díaz et al.* [2007] along the Galicia margin. Changes in the phase relationship between the tremor and tides presumably are induced by the opening or closing of certain pathways, perhaps in response to static deformation, ground shaking or mineral precipitation.

[40] The influence of tidal amplitude on tremor occurrence is examined by binning the number of events as a function of the tidal amplitude during the half-cycle in which it occurred. Figure 8d depicts tremor activity from stations 4 and 9 as well as a composite of all data from all stations. Regardless of whether tremor occurs dominantly during times of compression or extension, the number of detections increases approximately linearly with increasing trough-to-peak tidal strain amplitudes, ranging from ~0.6 events/h to ~1.3 events/h for tidal strain amplitudes between 0.25×10^{-8} and 4.5×10^{-8}. For comparison, the average tremor occurrence rate throughout the deployments is approximately 1 event/h. If the data are expressed in terms of tremor duration or amplitude, an equivalent linear relationship is observed with respect to increasing tidal amplitudes.

5.2. Preeruptive and Posteruptive Tremor Activity

[41] In volcanic systems, the abundance and character of tremor has been shown to vary in response to changing boundary conditions and eruptive
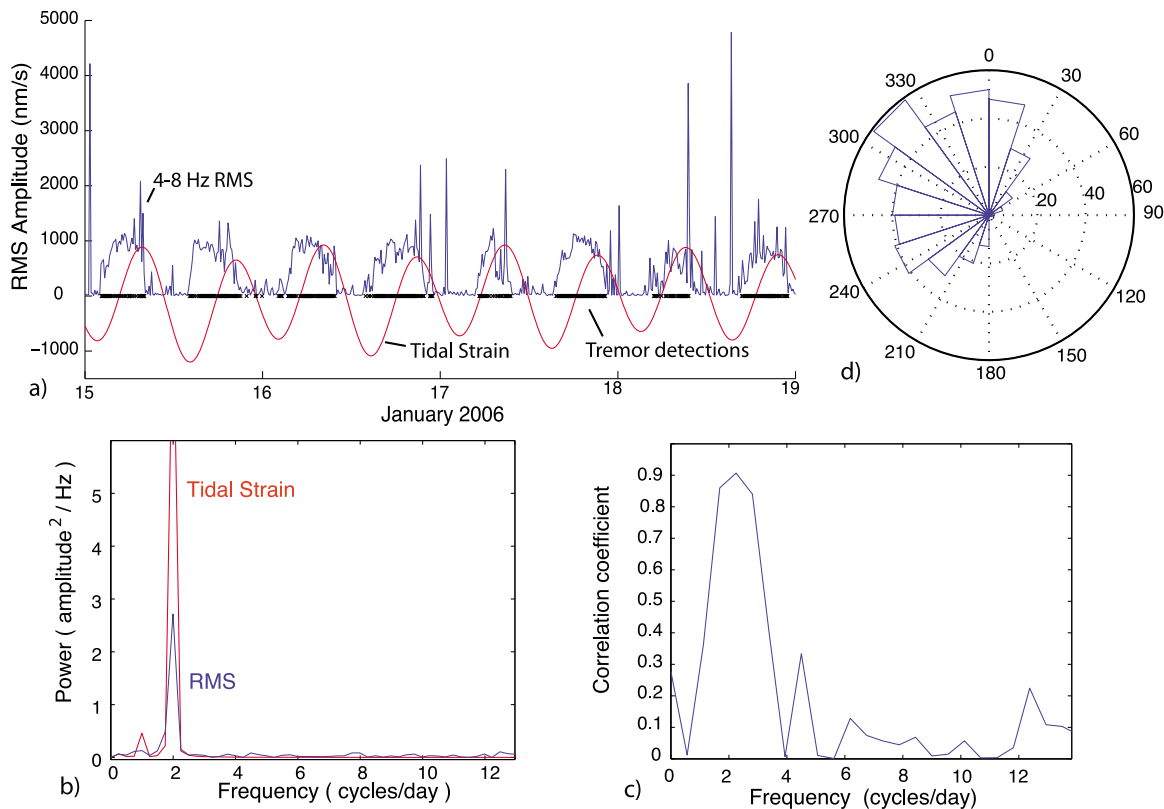
Figure 7. An example of a 4 day interval with a high correlation between RMS amplitudes and tidal strain. All of the data presented were recorded by on-axis station 9 between 15 and 19 January 2006 (deployment 3). (a) RMS velocity amplitude shown in blue. Tidal strain is plotted in red and ranges $\pm 2.5 \times 10^{-8}$. Tremor detections are plotted as individual crosses. (b) Fast Fourier transform (FFT) of tidal strain (red) and RMS amplitude (blue), both exhibiting peak spectral power at ~2 cycles/d. (c) Cross-spectral power analysis shows RMS amplitude and tidal strain exhibit 0.91 correlation at the frequency of 2 cycles/d. (d) Rose diagram depicting the tidal phase associated with each of the 489 tremor events plotted in Figure 7a. The mean phase angle is 307° with a Schuster p value of ≪0.001 (significant nonrandom temporal occurrence).

activity. The broadband spectral content of the OBS recordings is depicted in Figure 9, using daily averages for the three eruption-surviving stations (4, 5, and 9). Prior to 22 January 2006, 4–8 Hz tremor is evident at each station. During deployment 3, there is a small decrease in tremor frequency at station 4 (off axis) and slight increases at stations 5 and 9. However, within the context of the entire monitoring period, these fluctuations at a time scale of several months cannot be considered unusual. Stations 5 and 9 exhibit a divergence in the fundamental frequency beginning in the summer of 2005 (Figure 9). Throughout the entire 41 month period of monitoring, there is only one other instance (station 8, April–July 2004) where two distinct tremor bands are sustained within the 4–8 Hz frequency range for a significant period of time. *Kovachev et al.* [1997] has suggested that in low current environments (<4 cm/s) noise arises primarily due to the resonance of the OBS frame and components, predicting stable frequencies that

do not depend on the velocity of the currents. Consequently, the observed changes in frequency content through time further argue against a current driven noise source.

[42] For stations in proximity to the ridge crest (5 and 9), tremor activity within these same spectral bands continues following the 22 January eruptive event. Median tremor amplitudes decrease on both stations 5 and 9 after 22 January, from 266.71 and 896.79 to 237.85 and 768.10 nm/s, respectively. Tremor duration also decreases following the eruption at station 9, from 27.05 to 21.69 d/yr, but increases at station 5 from 17.56 d/yr to 21.13 d/yr. Off axis, however, there is a hiatus in activity, with no detections observed at station 4 until 25 February 2006. These events, which occur coinciding with a slight increase in local earthquake activity, contribute little power to the daily averaged spectra (Figure 9). During the 4th deployment (April 2006 to February 2007, not shown in Figure 9) more
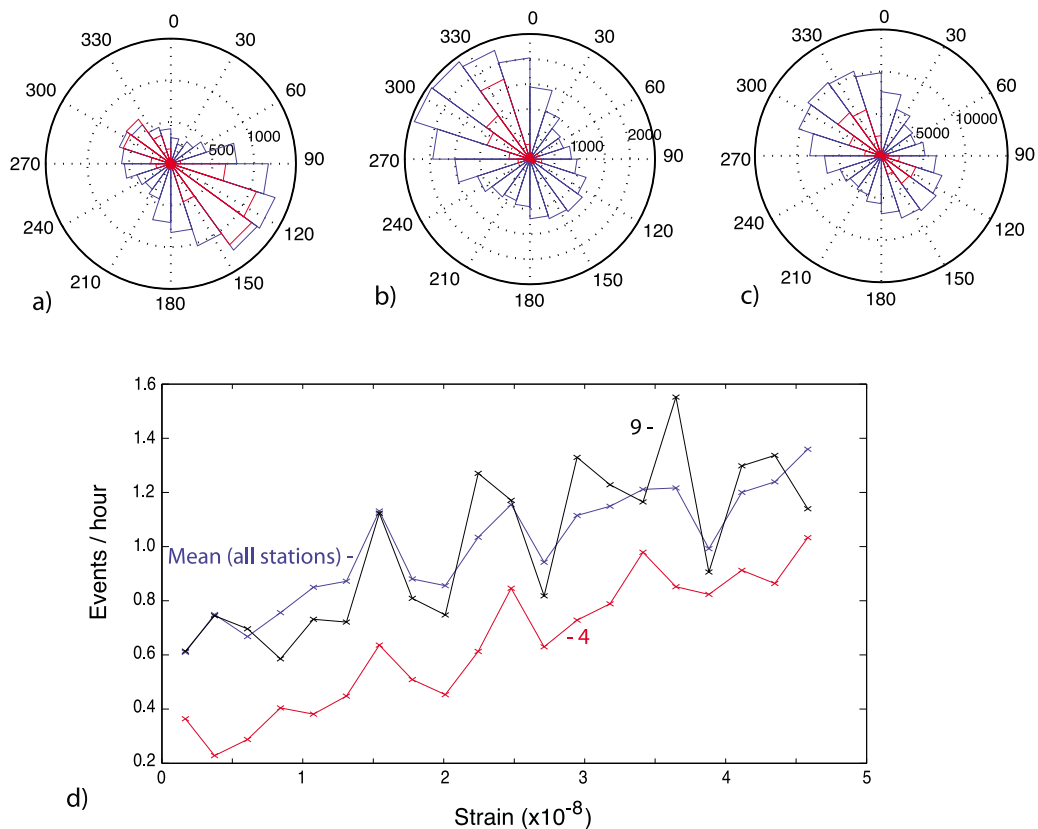
Figure 8. Rose diagrams depicting the phase of each Ishmael-detected tremor (blue) and RMS phase lag for all 4 day periods exhibiting a correlation >0.5 (red). The latter is scaled 60X. (a) Tremor activity at station 4, which peaks during periods of compressional strain, with a mean resultant phase angle of 139°. (b) Tremor recorded at station 9, with a mean resultant phase of 307°. (c) A composite of tremor activity from all stations with tremor occurrence dominantly during periods of both increasing extensional and compressional strain. (d) Tremor occurrence rates for stations 4 (red) and 9 (black) and a mean of all stations (blue). Occurrence rates were binned based on the strain amplitude during the tidal half-cycle in which the event occurred and are normalized based on total time within each amplitude bin. Tremor amplitude and duration (not shown) exhibit a similar positive linear trend with respect to increasing tidal amplitude.

robust tremor activity returns and the station records events at a rate of 6.01 d/yr, approaching the preeruptive average (9.05 d/yr) for deployment 3 (Table 1). During this time, the median RMS amplitudes for the tremor is 309 nm/s, versus 440 nm/s prior to 22 January (Table 1).

[43] Tremor energy release is spatially and temporally variable throughout the 41 month monitoring period (Figure 5), with no indication of a seasonal component that might indicate the influence of an external noise source. Roughly half of the deployed stations record a lull in tremor activity that extends throughout much of deployment 2 (Table 1 and Figure 5). The flux increases near the end of deployment 2 and into deployment 3 (April–May 2005), with the highest-amplitude tremor events recorded during the entire monitoring period observed at station 9 during May 2005

(Figure 5). During the roughly 2 month period before the 22 January 2006 spreading event, the energy flux associated with the tremor activity is relatively high on all three stations. However, higher levels are seen at other times during the study, and the predictive value of the energy flux time series in unclear (Figure 5).

[44] The scaling between cumulative tremor duration and amplitude has been used to characterize eruptive and noneruptive behavior within some terrestrial volcanic systems, as tremor amplitude is sensitive to variable pressures and source geometries [e.g., *Benoit et al.*, 2003]. This relationship is established by measuring the cumulative tremor duration at or above a given amplitude. The duration-amplitude distribution of tremor from this study is explored in Figure 10 in 3 month intervals selected to encompass periods with similar scaling
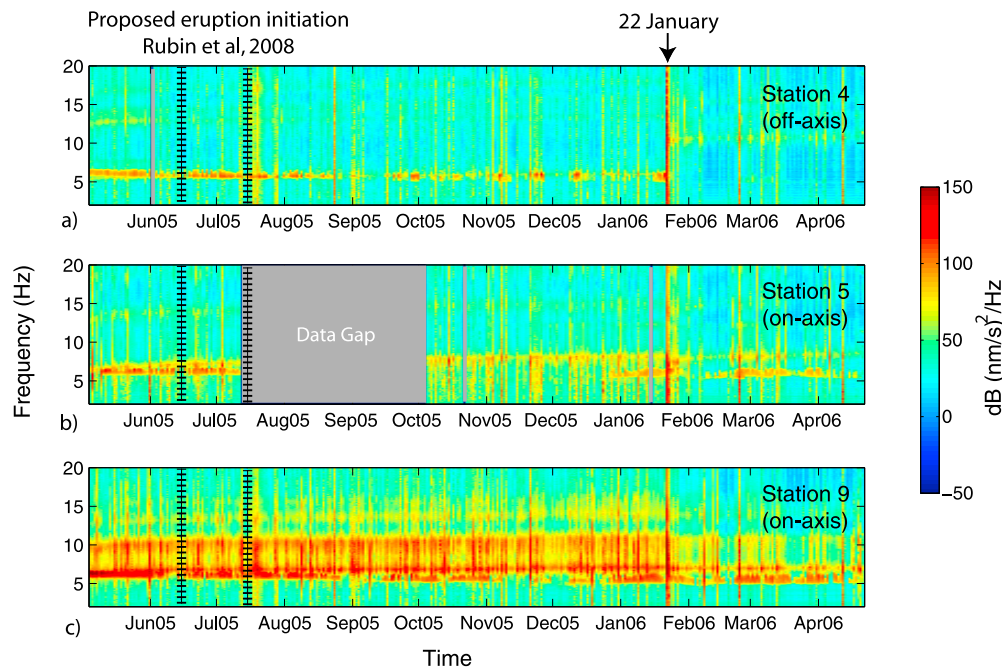
Figure 9. Average daily spectral signature for the three eruption surviving (deployment 3) stations: (a) station 4 off axis, (b) station 5 on axis, and (c) station 9 on axis. Each vertical slice represents the average spectral signal from one 24 h monitoring period, which is established using Welch's method with 1 h nonoverlapping windows. Gray shaded areas represent gaps in data coverage. The large amplitude broadband signals observed on 22 January 2006 are unique to all four deployments and have been interpreted to represent brittle failure in response to dike intrusion [*Tolstoy et al.*, 2006]. Notably, there is no 6 Hz tremor immediately following the eruption at station 4.

behaviors. Since these signals cannot be located, no distance attenuation correction is applied to the amplitude measurements [e.g., *McNutt*, 1992; *Nishimura et al.*, 1995; *Benoit et al.*, 2003]; however, they do provide relative measure of the changes observed at each station.

[45] This representation of the data indicates that all of the surviving deployment 3 stations exhibit their highest rate of tremor occurrence (cumulative d/yr) between May and July 2005 (Figure 10). The stations in closest proximity to the ridge axis (5 and 9) also exhibit their highest amplitudes during this time period, with the shape of the duration-amplitude distribution approaching the scale-bounded exponential model used to describe both volcanic [e.g., *Benoit et al.*, 2003] and non-volcanic [e.g., *Watanabe et al.*, 2007] tremor in other systems. This corresponds with the period of greatest energy release for stations 5 and 9 (Figure 5). For these on-axis stations, high-amplitude tremor disappears after roughly August 2005, with a similar duration-amplitude scaling observed for activity before and after the 22 January 2006 earthquake swarm (Figure 10).

[46] Off axis, station 4 exhibits a consistent duration-amplitude distribution between May 2005 and

the eruption on 22 January 2006, with an exponential scaling matching that seen during the May through July time frame for the on-axis stations. During deployment 3, the posteruptive rate of activity is low. When activity returns at a higher rate during deployment 4, the population shows reduced tremor amplitude and a scaling pattern similar to that seen on the near axis station during the period prior to the 22 January swarm.

[47] On a shorter time scale, beginning on 10 January 2006, the 4–8 Hz RMS amplitudes at stations 5 and 9 (on axis) exhibit a phase-shifted correlation with the tidal time series that exceeds 90%. This behavior persists through 18 and 20 January (Figure 11). Throughout the entire 41 month study, this is the only period longer than 4 days when the correlation coefficients at any station reach this threshold. Station 4, which lies on the near-axis flanks, does not exhibit an increased correlation (Figure 11).

[48] While 90% of tremor events range in duration between 28 and 200 s, posteruption (deployment 4) station 10 exhibits numerous events of duration longer than 1 h. During the heightened tremor-tidal correlation between 10 and 20 January 2006, on-axis station 9 is the only station to record an event
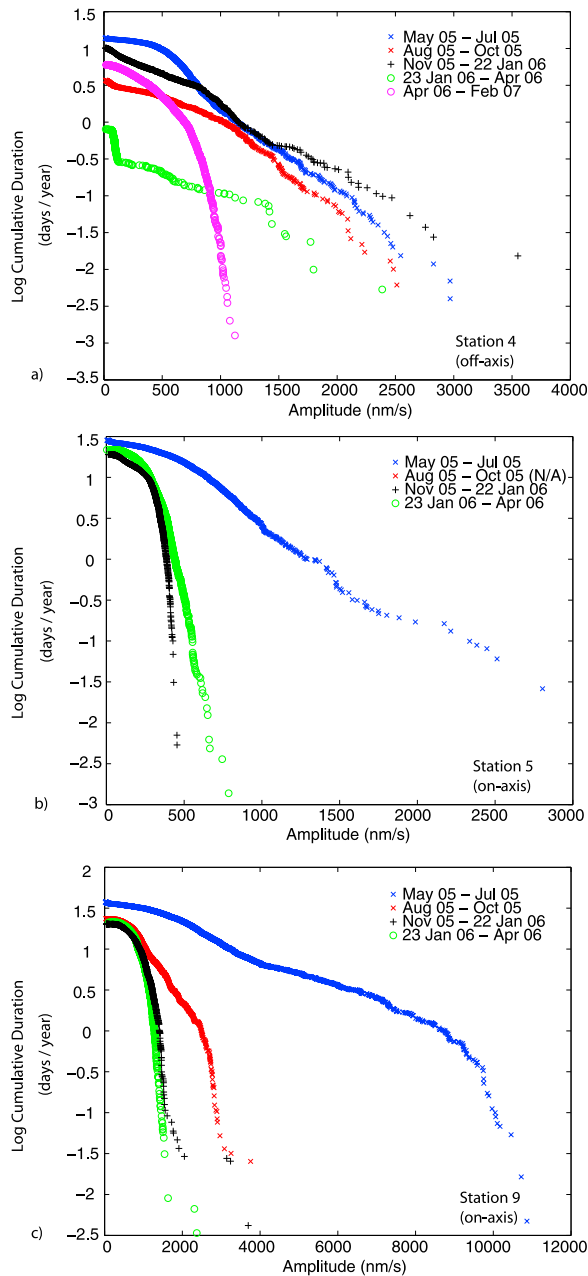
Figure 10. Duration-amplitude distributions of deployment 3 tremor activity recorded at stations (a) 4, (b) 5, and (c) 9. Blue represents activity between May and July 2005. Red represents activity between August 2005 and October 2005, during which time there are no data available for station 5. Black denotes the period between November 2005 and 22 January 2006, with the activity between 23 January and April 2006 shown in green. For station 4, which was reoccupied during the 4th deployment, data from April 2006 to February 2007 are also shown in magenta. Durations have been normalized based on the length of each monitoring period and are in units of cumulative days of tremor per year of observation.

preeruption of this duration. Station 12, which lies near the ridge axis recorded one such event postereruption and station 10 records a series of these events (31 total), with the longest detected event at over 4 h duration.

6. Discussion

[49] During most of the 41 month monitoring period, 4–8 Hz tremor signals are ubiquitous throughout the OBS array; however, neither the tremor waveforms, nor their envelopes, can be correlated between closely spaced (<1 km) stations. Because the axial magma lens lies roughly equidistant to all stations (∼1.4 km below the seafloor) [*Kent et al.*, 1993], this noncorrelation implies that the movement of magma and resonance within the chamber are unlikely mechanisms, as sources at such depths would be expected to produce coherent arrivals across the small-aperture array. Rather, the spatially heterogeneous nature of these signals suggests that multiple, small-amplitude sources are positioned within a few hundred meters of each OBS.

[50] Locally produced tremor activity exhibiting similar characteristics were observed during previous ocean bottom studies and these observations argue for a common source mechanism related to the movement of fluids at shallow depths. For example, observations from Axial Volcano [*Tolstoy et al.*, 2002] and the Galicia Margin [*Díaz et al.*, 2007] indicate monochromatic (∼6 Hz) and polychromatic (4–10 Hz fundamental) tremor signals that appear uncorrelated between OBS stations deployed with a separation of ∼5 km. Similarly, at Brothers Volcano, *Dziak et al.* [2008] describe polychromatic (3 Hz fundamental) tremor that cannot be correlated at stations separated by as little as 2 km. The tremor signals produced at these sites also exhibit temporal changes in frequency content and/or spectral gliding, consistent with 9°50'N activities. Waveform polarization measurements (deployments 3 and 4) show one or two dominant signal azimuths at each station, with polarization directions that cannot be aligned to a common source (Figure 3). *Díaz et al.* [2007] also observed consistent polarization signatures on the passive Galicia Margin.

[51] Tidal loading has been modeled to generate vertical and horizontal pressure gradients in hydrothermal systems as a result of spatial variations in fluid temperatures and crustal properties [*Crone and Wilcock*, 2005]. As a result, fluid velocities in
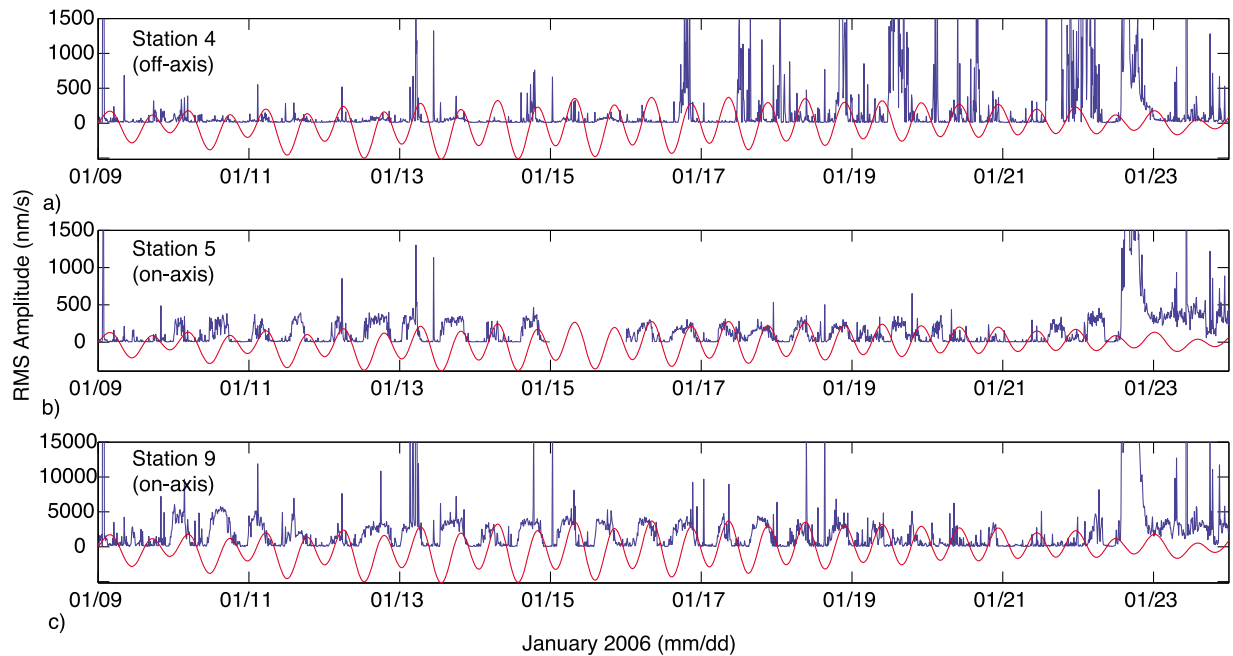
Figure 11. The 10 min RMS amplitudes in the 4−8 Hz band, plotted in blue, for stations (a) 4, (b) 5, and (c) 9 in the 2 weeks preceding the 22 January 2006 microearthquake swarm [*Tolstoy et al.*, 2006]. Tidal strain is plotted in red and ranges $\pm 2.5 \times 10^{-8}$. Beginning on 10 January, the phase-shifted correlation between the RMS velocity amplitudes and the tidal time series are greater than 0.90 for station 5 (through 18 January) and station 9 (through 20 January).

the seafloor are predicted to vary substantially with the tides [*Schultz and Elderfield*, 1997]. Tide-related variability has been observed at TAG hydrothermal system along the Mid-Atlantic Ridge in which fluid release pulses were correlated with tidal strain transients [*Fujioka et al.*, 1997]. Similarly, high-temperature fluid releases have been observed along the South Mariana Trough in response to peaks in ocean tidal loading [*Sato et al.*, 1995].

[52] For each of the 9°50′N stations, a semidiurnal (~12 h) periodicity in tremor occurrence is observed. Increased activity occurs either during times of increasing or decreasing tidal strain, typically reaching peak levels a few hours before the times of maximum extension or maximum compression. This pattern differs from that of tidally influenced microearthquake occurrence, which is characterized by increased activity surrounding the times of peak extensional stress [*Stroup et al.*, 2007], with poroelastic effects generating minor spatial variability in the mean phase angle (±10−20°) [*Stroup et al.*, 2009]. Hence, the timing of the observed tremor signals appears inconsistent with a Coulomb failure model, whereby tremor is generated within the fault zone during

episodes of slip [e.g., *Shelly et al.*, 2007; *Nakata et al.*, 2008].

[53] A semidiurnal periodicity in tremor occurrence also has been observed on Axial Volcano [*Tolstoy et al.*, 2002], although correlation with a specific tidal phase has not been analyzed in detail. On the Galicia Margin, however, *Díaz et al.* [2007] presented a detailed assessment of tremor occurrence with respect to a time series of sea surface height, which can be shown to dominate the tidal strain in that region. As observed for the 9°50′N data, they report tremor production during times of increasing and decreasing strain; however, those data exhibit a 6 h periodicity with elevated activity during each successive phase of tidal-induced compression and extension. The mechanisms controlling these different behaviors are not well understood, but may reflect changes in the local hydrology between an active ridge crest and highly sedimented passive margin.

[54] The spatial variability of tremor activity along the EPR ridge crest indicates that it is not likely to result from magmatic processes within the AMC. Rather, these tremor observations are consistent with fluid flow−induced oscillations [e.g., *Julian*, 1994] or resonance [*Chouet*, 1988] within a net-

work of shallow cracks. The temporal pattern of tremor activity strongly suggests that this fluid flow is driven by dynamic tidal strains and loading, with larger amplitude tides generating stronger tremor signals of longer duration (Figure 8).

[55] Earth tide induced extension, coupled with a small increase (typically < 20 cm) sea surface tidal height, should favor the movement of fluids into the crust. Whereas, crustal compression, coupled with a period of low ocean tide, should cause crustal fluids to be expelled. Microearthquake patterns and the distribution of vent sites have been used to establish that the overall pattern of hydrothermal circulation in the area is dominated by downwelling focused near an offset located at 9°49.25′N and upwelling beneath a high-temperature field centered near 9°50′N [Tolstoy et al., 2008]. However, with respect to its generation during times of increasing extension or compression, the pattern of tremor occurrence is more heterogeneous, suggesting that it is largely decoupled from this deeper pattern of hydrothermal circulation.

[56] Beginning in May 2005, stations 5 and 9 (on axis) exhibit a near simultaneous divergence into two frequency bands within the 4–8 Hz frequency range (Figure 9), with a drift in fundamental frequency observed on all three of the stations available for deployment 3. Small changes in the fundamental frequency could result from continued deformation of the upper crustal layer, resulting in a change in the dimensions of the conduit, or potentially a change in the temperature of the fluids within. Long-term changes in the tremor's fundamental frequency are observed at other times during the experiment; hence, these observations need not represent a precursor to the spreading event. More unusual is the formation of a second sustained tremor band in the 4–8 Hz range at both stations 5 and 9. This occurrence is interpreted to mark the opening of new cracks (source regions) or reopening of conduits previously sealed by mineral deposition. Also, during this period, the largest observed tremor amplitudes are recorded at station 9 (Figure 5), suggesting that the tremor (despite the upper crustal origin) may be tracking an early stage of preeruptive deformation. Volcanic deformation related to magma system pressurization is known to occur in the weeks and months preceding eruptive activity in subaerial settings [Dzurisin, 2007]. It often manifests through the opening of surface fractures or crustal dilations that may alter the geometry of fluid conduits and change the local hydrology [e.g., Brenguier et al., 2008].

[57] The changes in tremor characteristics at 9°50′N occur just before the onset of eruptive activity cited by Rubin et al. [2008] from the analysis of short half-life isotopes (late June through early July). However, as the close proximity of the stations to the axis favors the detection of submagnitude zero earthquakes [Bohnenstiehl et al., 2008], the absence of significant broadband microseismic activity is inconsistent with these changes marking the onset of eruptive activity (Figure 9). For significant magma to be extruded during this time, one or more dikes would have to propagate from the magma lens. While this may occur in the absence large earthquakes [e.g., Rubin and Gillard, 1998], any dike-induced change in stressing rate is expected to increase the local rate of earthquake production [Dieterich et al., 2000], and long-term monitoring shows that the region above of the AMC is not aseismic at the microseismic level [Sohn et al., 1998; Tolstoy et al., 2006].

[58] Within a time period of a few weeks before the 22 January 2006 swarm, on-axis tremor activity exhibits its highest correlation to tidal strain, with values above 90% correlation over an 8 day span (Figure 11). Coincident with this observation, temperature loggers in the high-temperature M vent (~9°51′N) record steadily decreasing temperatures on 9 January from background values of 360°C to values below the 150°C monitoring threshold over a period of less than 6 h (K. L. Von Damm et al., Vent fluid temperature time-series data and correlative data pre- and post-eruption for high-temperature vents at the East Pacific Rise 9°50′N, unpublished manuscript, 2009). Also during this time window, two regional hydrophones near 110°W, 8°N and 95°W, 8°N detected a series of ~250 small-magnitude (likely < 2.0 M) T wave signals [Dziak et al., 2009]. Although these events cannot be accurately located, they appear to be sourced in vicinity of the broader 9°50′N region. These observations suggest that there exists a precursory phase of deformation prior to rapid dike intrusion and eruption.

[59] In the days following the eruption, earthquake activity returns to background levels [Tolstoy et al., 2006; Dziak et al., 2009] and over the course of February, hydrothermal vent temperatures increase to values above background levels (Von Damm et al., unpublished manuscript, 2009). Tremor activity recorded on axis by eruption surviving stations depicts continued tremor activity at similar durations and amplitudes to those observed immediately prior to the eruption, while additional stations

deployed later along the ridge crest (deployment 4) provide evidence of extended tremor durations post-eruption. However, tremor activity off-axis is suspended for a month and does not return in earnest until April 2006 (Figures 9 and 10). The inferred diking event on 22 January 2006 [*Tolstoy et al.*, 2006] likely resulted in an input of heat energy and the opening of cracks and conduits as the dike cooled along the ridge axis, allowing for continued tremor activity and extended durations post-eruption immediately along the ridge axis. Off-axis however, tremor cessation is likely the result of the closure of cracks and conduits resulting from the stress field associated with dike injection [e.g., *Curewitz and Karson*, 1998]. Alternatively, maps of lava distribution indicate that flows extended off-axis, very near station 4 [*Soule et al.*, 2007]. If these flows remained unfractured for some period of time, they may have sealed existing conduits and altered the hydrology of the upper most crust.

7. Summary and Conclusions

[60] Tremor recorded along the EPR ridge crest exhibits a monochromatic or polychromatic spectral signature with a fundamental frequency near 6 Hz and individual tremor packets extending for 10s to 100s of seconds. Tremor occurrence and amplitude is heterogeneous throughout the array, implying multiple small amplitude sources in the vicinity of individual OBS stations. The spatial and temporal variability of tremor indicates it is likely the result of fluid flow in shallow subsurface cracks and conduits.

[61] Each of the 9°50′N stations exhibits a semidiurnal periodicity of tremor occurrence associated with increasing or decreasing tidal strain, with peak levels of tremor activity typically occurring a few hours before maximum compressional or extensional strain. This temporal pattern suggests that fluid flow in the shallow crust is driven by tidal strain transients, as larger tidal strains generate greater tremor occurrence with larger amplitudes and longer duration.

[62] Tremor rate and character also respond to the static magma induced deformation associated with eruptive activity. Deployments bracketing the eruption exhibit typically greater median RMS amplitudes and higher duration, resulting in increased energy flux. Tremor activity exhibits its greatest tidal correlations in the weeks preceding the eruption, which helps to define a 3 week precursory period that may signal imminent eruption on the ridge crest. Posteruption, a suspension of tremor activity off axis suggests the stress field associated with the dike injection or local lava flows closed cracks and conduits, while on-axis tremor continues with similar characteristics.

Acknowledgments

References

Adams, D. K., and L. S. Mullineaux (2008), Supply of gastropod larvae to hydrothermal vents reflects transport from local larval sources, *Limnol. Oceanogr.*, *53*(5), 1945–1955.

Benoit, J. P., S. R. McNutt, and V. Barboza (2003), Duration-amplitude distribution of volcanic tremor, *J. Geophys. Res.*, *108*(B3), 2146, doi:10.1029/2001JB001520.

Bohnenstiehl, D. R., F. Waldhauser, and M. Tolstoy (2008), Frequency-magnitude distribution of microearthquakes beneath the 9°50′N region of the East Pacific Rise, October 2003 through April 2004, *Geochem. Geophys. Geosyst.*, *9*, Q10T03, doi:10.1029/2008GC002128.

Brenguier, F., N. M. Shapiro, M. Campillo, V. Ferrazzini, Z. Duputel, O. Coutant, and A. Nercessian (2008), Towards forecasting volcanic eruptions using seismic noise, *Nat. Geosci.*, *1*, 126–130, doi:10.1038/ngeo104.

Brown, K. M., M. D. Tryon, H. R. DeShon, L. M. Dorman, and S. Y. Schwartz (2005), Correlated transient fluid pulsing and seismic tremor in the Costa Rica subduction zone, *Earth Planet. Sci. Lett.*, *238*(1–2), 189–203, doi:10.1016/j.epsl.2005.06.055.

Carton, H., et al. (2008), Characteristics of the crustal magma body in the 2005–2006 eruption area at 9°50′N on the East Pacific Rise from a 3D multi-channel seismic investigation, *Eos Trans. AGU*, *89*(53), Fall Meet. Suppl., Abstract B23F-03.

Chouet, B. (1988), Resonance of a fluid-driven crack: Radiation properties and implications for the source of long-period events and harmonic tremor, *J. Geophys. Res.*, *93*(B5), 4375–4400, doi:10.1029/JB093iB05p04375.

Chouet, B. (1996), Long-period volcano seismicity: Its source and use in eruption forecasting, *Nature*, *380*, 309–316, doi:10.1038/380309a0.

Chouet, B. (2003), Volcano seismology, *Pure Appl. Geophys.*, *160*, 739–788, doi:10.1007/PL00012556.

Cochran, E. S., J. E. Vidale, and S. Tanaka (2004), Earth tides can trigger shallow thrust fault earthquakes, *Science*, *306*(5699), 1164–1166, doi:10.1126/science.1103961.

Crone, T. J., and W. S. D. Wilcock (2005), Modeling the effects of tidal loading on mid-ocean ridge hydrothermal systems, *Geochem. Geophys. Geosyst.*, *6*, Q07001, doi:10.1029/2004GC000905.

Curewitz, D., and J. A. Karson (1998), Geological consequences of dike intrusion at mid-ocean ridge spreading centers, in *Faulting and Magmatism at Mid-Ocean Ridges*, *Geophys. Monogr. Ser.*, vol. 106, edited by W. R. Buck et al., pp. 117–136, AGU, Washington, D. C.

Díaz, J., J. Gallart, and O. Gaspa (2007), Atypical seismic signals at the Galicia Margin, North Atlantic Ocean, related to the resonance of subsurface fluid-filled cracks, *Tectonophysics*, *433*(1–4), 1–13, doi:10.1016/j.tecto.2007.01.004.

Dieterich, J. H., V. Cayol, and P. Okubo (2000), The use of earthquake rate as a stress meter at Kilauea volcano, *Nature*, *408*, 457–460, doi:10.1038/35044054.

Duennebier, F. K., G. Blackinton, and G. Sutton (1981), Current-generated noise recorded on ocean bottom seismometers, *Mar. Geophys. Res.*, *5*(1), 109–115, doi:10.1007/BF00310316.

Dziak, R. P., and C. G. Fox (2002), Evidence of harmonic tremor from a submarine volcano detected across the Pacific Ocean basin, *J. Geophys. Res.*, *107*(B5), 2085, doi:10.1029/2001JB000177.

Dziak, R. P., J. H. Haxel, H. Matsumoto, T. K. Lau, S. G. Merle, C. E. J. de Ronde, R. W. Embley, and D. K. Mellinger (2008), Observations of regional seismicity and local harmonic tremor at Brothers volcano, south Kermadec arc, using an ocean bottom hydrophone array, *J. Geophys. Res.*, *113*, B08S04, doi:10.1029/2007JB005533.

Dziak, R. P., D. R. Bohnenstiehl, H. Matsumoto, M. J. Fowler, J. H. Haxel, M. Tolstoy, and F. Waldhauser (2009), January 2006 seafloor-spreading event at 9°50′N, East Pacific Rise: Ridge dike intrusion and transform fault interactions from regional hydroacoustic data, *Geochem. Geophys. Geosyst.*, *10*, Q06T06, doi:10.1029/2009GC002388.

Dzurisin, D. (2007), *Volcano Deformation: Geodetic Monitoring Techniques*, 441 pp., Springer, Berlin.

Emter, D. (1997), Tidal triggering of earthquakes and volcanic events, in *Tidal Phenomenon*, edited by H. Wilhelm et al., pp. 293–309, Springer, Berlin.

Endo, E. T., and T. Murray (1991), Real-time seismic amplitude measurement (RSAM): A volcano monitoring and prediction tool, *Bull. Volcanol.*, *53*(7), 533–545, doi:10.1007/BF00298154.

Farrell, W. E. (1972), Earth tides, ocean tides and tidal loading, *Philos. Trans. R. Soc. London*, *274*(1239), 253–259, doi:10.1098/rsta.1973.0050.

Fornari, D. J., R. M. Haymon, M. R. Perfit, T. K. P. Gregg, and M. H. Edwards (1998a), Axial summit trough of the East Pacific Rise 9°–10°N: Geological characteristics and evolution of the axial zone on fast spreading mid-ocean ridges, *J. Geophys. Res.*, *103*(B5), 9827–9855, doi:10.1029/98JB00028.

Fornari, D. J., T. Shank, K. L. Von Damm, T. K. P. Gregg, M. Lilley, G. Levai, A. Bray, R. M. Haymon, M. R. Perfit, and R. Lutz (1998b), Time-series temperature measurements at high-temperature hydrothermal vents, East Pacific Rise 9°49′–51′N: Evidence for monitoring a crustal cracking event, *Earth Planet. Sci. Lett.*, *160*(3–4), 419–431, doi:10.1016/S0012-821X(98)00101-0.

Fox, C. G., H. Matsumoto, and T.-K. A. Lau (2001), Monitoring Pacific Ocean seismicity from an autonomous hydrophone array, *J. Geophys. Res.*, *106*(B3), 4183–4206, doi:10.1029/2000JB900404.

Fujioka, K., K. Kobayashi, K. Kato, M. Aoki, K. Mitsuzawa, M. Kinoshita, and A. Nishizawa (1997), Tide-related variability of TAG hydrothermal activity observed by deep-sea monitoring system and OBSH, *Earth Planet. Sci. Lett.*, *153*(3–4), 239–250, doi:10.1016/S0012-821X(97)00174-X.

Haxel, J. H., and R. P. Dziak (2005), Evidence of explosive seafloor volcanic activity from the Walvis Ridge, South Atlantic Ocean, *Geophys. Res. Lett.*, *32*, L13609, doi:10.1029/2005GL023205.

Haymon, R. M., D. J. Fornari, M. H. Edwards, S. Carbotte, D. Wright, and K. C. Macdonald (1991), Hydrothermal vent distribution along the East Pacific Rise crest (9°09′–54′N) and its relationship to magmatic and tectonic processes on fast-spreading mid-ocean ridges, *Earth Planet. Sci. Lett.*, *104*(2–4), 513–534, doi:10.1016/0012-821X(91)90226-8.

Haymon, R. M., et al. (1993), Volcanic eruption of the mid-ocean ridge along the East Pacific Rise crest at 9°45–52′N: Direct submersible observations of seafloor phenomena associated with an eruption event in April, 1991, *Earth Planet. Sci. Lett.*, *119*(1–2), 85–101, doi:10.1016/0012-821X(93)90008-W.

Julian, B. R. (1994), Volcanic tremor: Nonlinear excitation by fluid flow, *J. Geophys. Res.*, *99*(B6), 11,859–11,877, doi:10.1029/93JB03129.

Kent, G. A., A. J. Harding, and J. A. Orcutt (1993), Distribution of magma beneath the East Pacific Rise between the Clipperton transform and the 9°17′N Deval from forward modeling of common depth point data, *J. Geophys. Res.*, *98*(B8), 13,945–13,970, doi:10.1029/93JB00705.

Konstantinou, K. I., and V. Schlindwein (2003), Nature, wavefield properties and source mechanism of volcanic tremor: A review, *J. Volcanol. Geotherm. Res.*, *119*(1–4), 161–187, doi:10.1016/S0377-0273(02)00311-6.

Kovachev, S. A., T. A. Demidova, and A. V. Son'kin (1997), Properties of noise registered by pop-up ocean-bottom seismometers, *J. Atmos. Oceanic Technol.*, *14*, 883–888, doi:10.1175/1520-0426(1997)014<0883:PONRBP>2.0.CO;2.

Leet, R. C. (1988), Saturated and subcooled hydrothermal boiling in groundwater flow channels as a source of harmonic tremor, *J. Geophys. Res.*, *93*(B5), 4835–4849, doi:10.1029/JB093iB05p04835.

Madsen, P. T. (2005), Marine mammals and noise: Problems with root mean square sound pressure levels for transients, *J. Acoust. Soc. Am.*, *117*(6), 3952–3957, doi:10.1121/1.1921508.

Matsumoto, K., T. Takanezawa, and M. Ooe (2000), Ocean tide models developed by assimilating TOPEX/POSEIDON altimeter data into hydrodynamic model: A global model and a regional model around Japan, *J. Oceanogr.*, *56*, 567–582, doi:10.1023/A:1011157212596.

Matsumoto, K., T. Sato, T. Takanezawa, and M. Ooe (2001), Gotic2: A program for computation of oceanic tidal loading effect, *J. Geod. Soc. Jpn.*, *47*, 243–248.

McNutt, S. R. (1992), Volcanic tremor, in *Encyclopedia of Earth System Science*, vol. 4, pp. 417–425, Academic, San Diego, Calif.

McNutt, S. R. (2005), Volcanic seismology, *Annu. Rev. Earth Planet. Sci.*, *33*, 461–491, doi:10.1146/annurev.earth.33.092203.122459.

Mellinger, D. K. (2001), Ishmael 1.0 user's guide, *NOAA Tech. Memo. OAR PMEL-120*, Pac. Mar. Environ. Lab., NOAA, Seattle, Wash.

Mellinger, D. K., and C. W. Clark (2000), Recognizing transient low-frequency whale sounds by spectrogram correlation, *J. Acoust. Soc. Am.*, *107*(6), 3518–3529, doi:10.1121/1.429434.

Miller, M. M., T. Melbourne, D. J. Johnson, and W. Q. Sumner (2002), Periodic slow earthquakes from the Cascadia subduction zone, *Science*, *295*(5564), 2423, doi:10.1126/science.1071193.

Nakata, R., N. Suda, and H. Tsuruoka (2008), Non-volcanic tremor resulting from the combined effect of the Earth tides and slow slip events, *Nat. Geosci.*, *1*(10), 676–678, doi:10.1038/ngeo288.

Nishimura, T., H. Hamaguchi, and S. Ueki (1995), Source mechanisms of volcanic tremor and low-frequency earthquakes associated with the 1988–89 eruptive activity of Mt Tokachi, Hokkaido, Japan, *Geophys. J. Int.*, *121*(2), 444–458, doi:10.1111/j.1365-246X.1995.tb05725.x.

Obara, K. (2002), Nonvolcanic deep tremor associated with subduction in southwest Japan, *Science*, *296*(5573), 1679–1681, doi:10.1126/science.1070378.

Obara, K., H. Hirose, F. Yamamizu, and K. Kasahara (2004), Episodic slow slip events accompanied by non-volcanic tremors in southwest Japan subduction zone, *Geophys. Res. Lett.*, *31*, L23602, doi:10.1029/2004GL020848.

Piccinini, D., and G. Saccorotti (2008), First observations of non-volcanic, long-period seismicity in the central Apennines, Italy, *Geophys. Res. Lett.*, *35*, L12303, doi:10.1029/2008GL034120.

Pontoise, B., and Y. Hello (2002), Monochromatic infra-sound waves recorded offshore Ecuador: Possible evidence of methane release, *Terra Nova*, *14*(6), 425–435, doi:10.1046/j.1365-3121.2002.00437.x.

Rogers, G., and H. Dragert (2003), Episodic tremor and slip on the Cascadia subduction zone: The chatter of silent slip, *Science*, *300*(5627), 1942–1943, doi:10.1126/science.1084783.

Rubin, A. M., and D. Gillard (1998), Dike-induced earthquakes: Theoretical considerations, *J. Geophys. Res.*, *103*, 10,017–10,030.

Rubin, K. H., J. D. Mcdougall, and M. R. Perfit (1994), ²¹⁰Po-²¹⁰Pb dating of recent volcanic eruptions on the sea floor, *Nature*, *368*, 841–844, doi:10.1038/368841a0.

Rubin, K. H., M. Tolstoy, D. J. Fornari, R. P. Dziak, S. A. Soule, F. Waldhauser, and K. L. Von Damm (2008), Integrating radiometric, geophysical and thermal signals of volcanic unrest and eruption in 2005–06 at 9°50′N EPR, *Eos Trans. AGU*, *89*, Fall Meet. Suppl., Abstract B23F-07.

Rubinstein, J. L., M. La Rocca, J. E. Vidale, K. C. Creager, and A. G. Wech (2008), Tidal modulation of nonvolcanic tremor, *Science*, *319*(5860), 186–189, doi:10.1126/science.1150558.

Sato, T., J. Kasahara, and K. Fujioka (1995), Observation of pressure change associated with hydrothermal upwelling at a seamount in the South Mariana Trough using an ocean bottom seismometer, *Geophys. Res. Lett.*, *22*(11), 1325–1328, doi:10.1029/95GL01314.

Scheirer, D. S., T. M. Shank, and D. J. Fornari (2006), Temperature variations at diffuse and focused flow hydrothermal vent sites along the northern East Pacific Rise, *Geochem. Geophys. Geosyst.*, *7*, Q03002, doi:10.1029/2005GC001094.

Schultz, A., and H. Elderfield (1997), Controls on the physics and chemistry of seafloor hydrothermal circulation, *Philos. Trans. R. Soc. London*, *355*, 387–425, doi:10.1098/rsta.1997.0014.

Shank, T. M., D. J. Fornari, K. L. Von Damm, M. D. Lilley, R. M. Haymon, and R. A. Lutz (1998), Temporal and spatial patterns of biological community development at nascent deep-sea hydrothermal vents (9°50′N, East Pacific Rise), *Deep Sea Res., Part II*, *45*(1–3), 465–515, doi:10.1016/S0967-0645(97)00089-1.

Shelly, D. R., G. C. Beroza, and S. Ide (2007), Complex evolution of transient slip derived from precise tremor locations in western Shikoku, Japan, *Geochem. Geophys. Geosyst.*, *8*, Q10014, doi:10.1029/2007GC001640.

Sohn, R. A., D. J. Fornari, K. L. Von Damm, J. A. Hildebrand, and S. C. Webb (1998), Seismic and hydrothermal evidence for a cracking event on the East Pacific Rise crest at 9°50′N, *Nature*, *396*(6707), 159–161, doi:10.1038/24146.

Sohn, R. A., J. A. Hildebrand, and S. C. Webb (1999), A microearthquake survey of the high-temperature vent fields on the volcanically active East Pacific Rise (9°50′N), *J. Geophys. Res.*, *104*(B11), 25,367–25,378, doi:10.1029/1999JB900263.

Soule, S. A., D. J. Fornari, M. R. Perfit, and K. H. Rubin (2007), New insights into mid-ocean ridge volcanic processes from the 2005–2006 eruption of the East Pacific Rise, 9°46′N–9°56′N, *Geology*, *35*(12), 1079–1082, doi:10.1130/G23924A.1.

Stroup, D. F., D. R. Bohnenstiehl, M. Tolstoy, F. Waldhauser, and R. T. Weekly (2007), Pulse of the seafloor: Tidal triggering of microearthquakes at 9°50′N East Pacific Rise, *Geophys. Res. Lett.*, *34*, L15301, doi:10.1029/2007GL030088.

Stroup, D. F., M. Tolstoy, T. J. Crone, A. Malinverno, D. R. Bohnenstiehl, and F. Waldhauser (2009), Systematic along-axis tidal triggering of microearthquakes observed at 9°50′N East Pacific Rise, *Geophys. Res. Lett.*, *36*, L18302, doi:10.1029/2009GL039493.

Talandier, J., and E. A. Okal (1987), Seismic detection of underwater volcanism: The example of French Polynesia, *Pure Appl. Geophys.*, *125*(6), 919–950, doi:10.1007/BF00879361.

Talandier, J., and E. A. Okal (1996), Monochromatic T waves from underwater volcanoes in the Pacific Ocean: Ringing witnesses to geyser processes, *Bull. Seismol. Soc. Am.*, *86*(5), 1529–1544.

Tanaka, S., M. Ohtake, and H. Sato (2002), Evidence for tidal triggering of earthquakes as revealed from statistical analysis of global data, *J. Geophys. Res.*, *107*(B10), 2211, doi:10.1029/2001JB001577.

Tolstoy, M., F. L. Vernon, J. A. Orcutt, and F. K. Wyatt (2002), Breathing of the seafloor: Tidal correlations of seismicity at Axial volcano, *Geology*, *30*(6), 503–506.

Tolstoy, M., et al. (2006), A seafloor spreading event captured by seismometers, *Science*, *314*, 1920–1922, doi:10.1126/science.1133950.

Tolstoy, M., F. Waldhauser, D. R. Bohnenstiehl, R. T. Weekly, and W.-Y. Kim (2008), Seismic identification of along-axis hydrothermal flow in the East Pacific Rise, *Nature*, *451*, 181–184, doi:10.1038/nature06424.

Von Damm, K. L., S. E. Oosting, R. Kozlowski, L. G. Buttermore, D. C. Colodner, H. N. Edmonds, J. M. Edmond, and J. M. Grebmeier (1995), Evolution of East Pacific Rise hydrothermal vent fluids following a volcanic eruption, *Nature*, *375*, 47–50, doi:10.1038/375047a0.

Waldhauser, F., and W. L. Ellsworth (2000), A double-difference earthquake location algorithm: Method and application to the Northern Hayward Fault, California, *Bull. Seismol. Soc. Am.*, *90*(6), 1353–1368, doi:10.1785/0120000006.

Watanabe, T., Y. Hiramatsu, and K. Obara (2007), Scaling relationship between the duration and the amplitude of non-volcanic deep low-frequency tremors, *Geophys. Res. Lett.*, *34*, L07305, doi:10.1029/2007GL029391.

Wilcock, W. S. D., S. D. Archer, and G. M. Purdy (2001), Microearthquakes on the Endeavour segment of the Juan de Fuca Ridge, *J. Geophys. Res.*, *107*(B12), 2236, doi:10.1029/2001JB000505.